

# Higgs Boson Discovery Potential of LHC in the Channel $pp \rightarrow \gamma\gamma + jet$

S. Abdullin<sup>‡</sup>, M. Dubinin<sup>\*</sup>, V. Ilyin<sup>\*</sup>,  
D. Kovalenko<sup>\*</sup>, V. Savrin<sup>\*</sup>, N. Stepanov<sup>‡</sup>

<sup>‡</sup> *Institute for Theoretical and Experimental Physics, 117259 Moscow, Russia*

<sup>\*</sup> *Institute of Nuclear Physics, Moscow State University, 119899 Moscow, Russia*

## Abstract

We discuss the SM Higgs discovery potential of LHC in the reaction  $pp \rightarrow H + jet \rightarrow \gamma\gamma + jet$  when the jet is observed at sufficiently high  $E_t$  to be reliably identified. We conclude that this channel gives promising discovery possibilities for the Higgs boson mass range 100-140 GeV, during LHC operation at a low luminosity. With  $30 \text{ fb}^{-1}$  of accumulated data and for  $M_H = 120 \text{ GeV}$  about 100 signal events could be observed with the number of background events larger by a factor of 2 only, showing a signal significance  $S/\sqrt{B} \sim 7$ . We use the difference of distributions in the partonic subprocess energy  $\sqrt{\hat{s}}$  for the signal and background for a better separation of the signal.

## Introduction

It is well known that the observation of Higgs boson with mass  $M_H < 140$  GeV at the LHC collider ( $pp, \sqrt{s} = 14$  TeV) in the inclusive channel  $pp \rightarrow \gamma\gamma + X$  is not easy [1, 2]. The  $\gamma\gamma$  continuum rapidly increases for smaller  $\gamma\gamma$  pair invariant masses, and it is necessary to separate a rather elusive Higgs boson signal from it. In this situation it is important to understand whether we can observe any other discovery channels. In this paper we are considering (in the Standard Model) the reaction  $pp \rightarrow H + jet \rightarrow \gamma\gamma + jet$  when Higgs boson is produced with large transverse momentum recoiling against a hard jet. Of course, in this channel the signal rate is much smaller in comparison with the inclusive  $pp \rightarrow \gamma\gamma + X$  case. At the same time, as we shall see below, the situation with the background is undoubtedly much better. We can usefully exploit richer kinematical features of the final state  $\gamma\gamma + jet$ , when some specific jet distributions in the partonic c.m.s. are different for signal and background processes.

The idea to look for Higgs boson associated with a high  $E_t$  jet in the final state was considered in [3]. In [4, 5] the corresponding subprocesses were calculated within the minimal supersymmetric extension of the Standard Model. However, in [4, 5] Higgs decay channels were not considered and in [3] only the final state  $\tau^+\tau^- + jet$  was analyzed. In [6] the SM heavy Higgs boson decay into the  $WW$  or  $ZZ$  pairs was discussed for  $H + jet$  production. Promising results have been obtained recently in [7] for  $\gamma\gamma + 2jets$  final state with two very forward jets ( $|\eta| < 5$ ). In [8] the final state  $\gamma\gamma + (\geq 2jets)$  was simulated in the realistic CMS detector environment. The final state  $\gamma\gamma + jet$  with only one high  $E_t$  jet recoiling against the Higgs boson has not been analyzed yet and we investigate it in detail <sup>1</sup>.

## 1. Calculation framework

We calculated cross sections and distributions by means of CompHEP package [10]. Methods of multichannel adaptive Monte Carlo integration over the phase space implemented in the package are described in [11].

The cross sections of signal subprocesses under discussion depend significantly on the choice of QCD parameters. There are three sources of this dependence: (1) QCD evolution of the parton distribution functions; (2)  $\alpha_s$  dependence in the subprocesses; (3)  $H \rightarrow \gamma\gamma$  branching variation due to QCD corrections to the  $\Gamma_H^{tot}$ . In the leading order the corresponding corrections can be factorized. Moreover, due to a very small value of  $\Gamma_H^{tot}$  for  $M_H < 140$  GeV the fixed value of strong coupling  $\alpha_s(M_H)$  can be used for the evaluation of  $H \rightarrow \gamma\gamma$  branching. However, it is well-known that for the reaction  $pp \rightarrow H \rightarrow \gamma\gamma$  the dependence on the renormalization scale  $\mu$  and on the parton factorization scale  $Q$  is strong enough, and the next-to-leading order analysis is necessary (see [12] and references therein). The NLO corrections decrease this  $(\mu, Q)$  theoretical uncertainty, showing only a  $\sim 15\%$  sensitivity of the final result. One can hope to observe a similar effect also for the case of Higgs boson production at high  $p_t$ . However, self-consistent analysis requires the NLO corrections to hard subprocesses which are not known yet, unfortunately<sup>2</sup>. Thus, today we made only the LO analysis when parton distribution functions and running  $\alpha_s$  in subprocesses are taken at the leading order. We used the parametrization CTEQ4l ( $\alpha_s(M_Z) = 0.1317$ ,  $\Lambda_{QCD}^{(5)} = 181$  MeV) [14]. At the same time QCD NLO formulas [15, 12] were used for the evaluation of  $\Gamma_H^{tot}$  with the reference value  $Br(H \rightarrow \gamma\gamma) = 1.534 \cdot 10^{-3}$  at  $M_H = 100$  GeV. Parameter values used in our analysis are  $M_Z = 91.187$  GeV,  $\sin\theta_w = 0.4732$ , and  $m_s = 0.2$  GeV,  $m_c = 1.42$  GeV,  $m_b = 4.62$  GeV,  $m_t = 175$  GeV.

Typical acceptances of the LHC detectors ATLAS and CMS should be taken into account in the analysis. For photons we are using the cuts similar to already well analysed cuts of the

---

<sup>1</sup>Primary analysis of the reaction  $pp \rightarrow \gamma\gamma + jet$  can be found in [9], where we also considered the processes  $pp \rightarrow WH, t\bar{t}H \rightarrow \gamma\gamma + lepton$ .

<sup>2</sup>Recently formulas for the corresponding virtual corrections were calculated in the  $m_t \rightarrow \infty$  limit [13].

inclusive channel [1, 2]: two photons are required with  $p_t^\gamma > 40$  GeV for each photon (somewhat harder than for the inclusive channel), and photon rapidity  $|\eta_\gamma| < 2.5$ . For a jet two sets of basic kinematical cuts will be discussed in further analysis:

$$\mathbf{C1}: E_t^{jet} > 40 \text{ GeV}, |\eta_{jet}| < 2.4; \quad \mathbf{C2}: E_t^{jet} > 30 \text{ GeV}, |\eta_{jet}| < 4.5.$$

The first set corresponds to the central part of calorimeter where a jet with transverse energy greater than 40 GeV can be detected with highest efficiency. The second set assumes forward parts of the hadron calorimeter involved. The analysis of background processes made for the inclusive channel has shown that photons should be isolated. So we apply the cut  $\Delta R > 0.3$  for each  $\gamma - \gamma$  and  $\gamma - g(q)$  pair, where  $\Delta R = \sqrt{\Delta\phi^2 + \Delta\eta^2}$  is the standard variable separating particles in the *azimuth angle - rapidity* plane.

## 2. Signal processes

There are three QCD subprocesses giving a signal from the Higgs boson in the channel under discussion:  $gg \rightarrow H + g$ ,  $gq \rightarrow H + q$  and  $q\bar{q} \rightarrow H + g$ . Feynman diagrams contributing in the leading order  $\alpha_s^3$  are shown in Fig. 1. The corresponding matrix elements were calculated analytically in [3] and we implemented these formulas in our code. We found that the  $gg \rightarrow H + g \rightarrow \gamma\gamma + g$  subprocess gives the main contribution to the signal rate. The  $gq$  channels with light quarks give 20-25% of the *gluon-gluon* signal contribution, while the  $q\bar{q}$  channels can be neglected. Furthermore, at large values of parton factorization scale,  $\sim 10^4$  GeV<sup>2</sup>, typical for intermediate Higgs boson production, one can expect noticeable contributions of the strange and heavy quark sea. We found that it gives 10% of the dominant *gluon-gluon* subprocess. Then, tree-level subprocess  $gg \rightarrow H + b + \bar{b}$ , where the Higgs boson is radiated from the final  $b$  quark or  $b$ -propagator, contributes to  $\gamma\gamma + jet$  signal events if we do not register (*veto*) the events with both  $b$  quark jets observed. We found that this process gives about 1.5% of the  $gg$  contribution. Finally we note that the s-channel subprocesses  $q\bar{q} \rightarrow H + Q + \bar{Q}$ , where  $q$  is a light quark and  $Q$  is  $b$  or  $t$  quark, are negligible. In total QCD subprocesses give 3.3 fb, 5.7 fb and 5.5 fb with the **C1** set of cuts for  $M_H = 100, 120$  and  $140$  GeV, correspondingly, and 5.5 fb, 10.6 fb and 9.8 fb with the **C2** set.

The second group of signal subprocesses includes the electroweak reactions of Higgs production through  $WW$  or  $ZZ$  fusion (Fig. 2a) with the high  $E_t$  jet in the final state from the scattered quark, and the Higgs boson production associated with  $W$  or  $Z$  (Fig. 2b) decaying into quark-antiquark pairs. Of course, if the signature with only one jet is under discussion, one should *veto* the second quark jet. The  $WW/ZZ$  fusion processes were calculated in [16], while the processes of  $HW/HZ$  associated production were considered in [17]. One should note that the contribution of these subprocesses decreases when we change **C1** set of cuts to **C2**, what is opposite to the case of QCD signal subprocesses. The reason is *veto* condition for one of the jets. Indeed, typical transverse momentum of the final quark (in the dominant  $WW/ZZ$  fusion production processes) is about half of the vector boson mass. So, weaker jet cut  $E_t > 30$  GeV in the *veto* condition removes a larger number of events. We found that the cross section of fusion processes is 2-3 times larger than for the processes of associated production. In EW channels  $s$  and  $c$  quark sea gives about 10% of  $u$  and  $d$  quark (valence plus sea) contribution. In total, EW processes give 1.0 fb, 1.6 fb and 1.5 fb with the **C1** set of cuts for  $M_H = 100, 120$  and  $140$  GeV, correspondingly, and 0.65 fb, 1.1 fb and 1.1 fb with the **C2** set. So the electroweak signal rate is on the level of 30% of the QCD signal with the **C1** set of cuts and 10% with the **C2** set.

## 3. Irreducible background processes

Let us now look at the irreducible background. Three subprocesses contribute here, two of them at the tree level,  $gq \rightarrow \gamma + \gamma + q$  (Fig. 3a) and  $q\bar{q} \rightarrow \gamma + \gamma + g$  (Fig. 3b), and the third one at the one loop level,  $gg \rightarrow \gamma + \gamma + g$ . The  $q\bar{q}$  channel with  $u$  and  $d$  quarks in the initial state

gives the cross section on the level 15-20% of the main irreducible background  $gq$  ( $q = u, d$ ) with the **C1** set of cuts, and 15-30% with the **C2** set for Higgs mass range 100-140 GeV. The contributions of strange and heavy quark sea in the initial state are on the level 25-30% of the main  $gq$  channel. Here about 85% of the contribution is coming from the  $c$  quark sea. The  $s$  quark contribution is suppressed by the factor 16 originating from a smaller fractional charge.

The matrix element for the one-loop process  $gg \rightarrow \gamma + \gamma + g$ , when the photons are radiated from the quark loop, is unknown yet. We estimated this cross section by means of PYTHIA [18] simulation, switching on the gluon bremsstrahlung from the initial state in the subprocess  $gg \rightarrow \gamma + \gamma$ . This is definitely only one of physical contributions to the one-loop process. The result of these simulations shows us that the one-loop background is about 2-4% of the main contribution coming from the  $gq$  channel. So we neglect the one-loop background in further analysis, however, this point is one of a serious theoretical uncertainties.

In total, the irreducible background contribution amounts to 9.3 fb, 13.7 fb and 16.1 fb in the 1 GeV bin around the values of  $M_{\gamma\gamma} = 100, 120$  and 140 GeV, correspondingly, and with the **C1** set of cuts. Of course, with the **C2** set of cuts the background is larger, the corresponding numbers are 15.3 fb, 25.3 fb and 25.1 fb in the 1 GeV bin.

## 4. Reducible background processes

Various processes could give a background due to radiation of photons from the fragmentating quarks or gluons. Photon production in a jet hadronization is also possible, and is defined in particular by a  $\pi^0$ -meson production. The energetic  $\pi^0$ 's, decaying mainly to a photon pair, can be detected as a single photon in the electromagnetic calorimeter. First kind of such reducible background is coming from the subprocesses  $gq \rightarrow \gamma + g + q$ ,  $gg \rightarrow \gamma + q + \bar{q}$  and  $qq' \rightarrow \gamma + q(g) + q'(g)$ , in the case when the final gluon or quark produces an energetic isolated photon but other products of hadronization escape the detection as a jet. One can say that *a jet is misidentified as a photon*. Second kind of reducible background could come from the subprocesses  $gq \rightarrow \gamma + q$ ,  $q\bar{q} \rightarrow \gamma + g$  when the second photon is produced in the quark or gluon fragmentation but other products of the hadronization are still detected as a jet with proper separation from this photon. Third source of reducible background is connected with the pure QCD subprocesses of  $2 \rightarrow 2$  and  $2 \rightarrow 3$  types, when all particles in the final state are gluons or quarks. We performed rough analysis of these QCD reducible backgrounds in [9] and found that they turn out to be less than 20% of the irreducible background, and the misidentification rate is given mainly by the processes of the first kind. Here we used the  $\gamma(\pi^0)/jet$  rejection factor equal to 2500 for a jet misidentified as a photon and 5000 for a well separated  $\gamma(\pi^0)$  production by a jet. These factors were obtained for a jet satisfying the cuts described above with the help of PYTHIA simulations. No additional  $\pi^0$  rejection algorithms were used.

## 5. Dependence on the $Q^2$ scale

In our calculations we used  $Q^2 = M_H^2 + 2(E_t^{jet})^2$  as the parton factorization scale and the normalization scale for running  $\alpha_s$  in the hard QCD signal subprocesses, as well as in the background processes. At the same time for the  $WW/ZZ$  fusion we used  $Q^2 = (M_V/2)^2$  ( $M_V = M_W, M_Z$ ) and  $Q^2 = (M_V + M_H)^2$  for the  $HW/HZ$  associated production. Certainly, due to  $\alpha_s^3$  order of partonic subprocesses one can expect strong dependence on the choice of  $Q^2$  for the QCD signal. We checked that for  $Q^2 = M_H^2$ , the corresponding signal cross section increases by 15%, while the background cross section increases only by  $\sim 5\%$ . If one uses  $Q^2 = (50\text{GeV})^2$ , the QCD signal cross section increases by 80% while the background only by 13%. Such strong  $Q^2$  dependence shows that the complete NLO analysis is needed.

## 6. Reconstruction of event kinematics

The distributions  $d\sigma/d\sqrt{s}$  in parton collision energy presented in Fig. 4 show that the back-

ground processes contribute at a smaller  $\sqrt{\hat{s}}$  in comparison with the QCD signal processes. So, one can hope that the corresponding cut can improve the  $S/B$  ratio. Photon energy can be measured with a high enough precision, so the main uncertainty of the  $\sqrt{\hat{s}}$  reconstruction is defined by the accuracy of a final parton energy and momentum reconstruction (see details in [1, 2]). The energy of a parton can be reconstructed with the accuracy  $(\delta E/E)^2 \sim 100\% \sqrt{E} \oplus 5\%$ . It means that for jets with transverse energy more than 30 GeV the parton energy will be reconstructed with the accuracy  $\sim 7$  GeV. Taking into account all factors, one can expect that  $\sqrt{\hat{s}}$  variable can be reconstructed with the error  $\sim 10$  GeV. It is clear from the distributions presented in Fig. 4 that such accuracy is good enough to apply a cut on  $\sqrt{\hat{s}}$  for the suppression of the background. However  $\delta E$  is mostly related to the energy loss due to the undetected products of hadron fragmentation. It follows that the experimental distributions can be shifted to the smaller  $\sqrt{\hat{s}}$  values in comparison with Fig. 4. But the scale of smearing in this distribution (more dangerous for our analysis) should be definitely smaller than 10 GeV. One should note that processes at higher order  $\alpha_s$  (contributing to the NLO corrections) have more than 3 particles in the partonic final state. So, strictly speaking, the energies and momenta of photons and the detected jet are not sufficient for the reconstruction of partonic c.m.s. collision energy in these events. However, one can hope that the main contribution to the QCD corrections should go from virtual and soft gluons and cannot affect significantly the reconstruction of  $\sqrt{\hat{s}}$  variable.

We found that the cut  $\sqrt{\hat{s}} > 210$  GeV decreases the QCD signal cross section only by 25-30% with the **C1** set of basic cuts, while the background is suppressed much stronger, for example by a factor of 2 when  $M_H = 120$  GeV. For the **C2** set of basic cuts the corresponding numbers are 20-35% decrease for the signal rate and suppression factor of 1.7-2.8 for the background. It means, for example, that with the **C2** set of cuts the  $S/B$  ratio is improved by a factor of  $\sim 2$  for  $M_H = 100 - 140$  GeV. One can get  $S/B$  even better by applying much stronger  $\hat{s}$  cut. For example  $\sqrt{\hat{s}} > 300$  GeV in the case of **C2** set suppresses the background by a factor of 8.7 while the QCD signal only by a factor of 2.6.

$M_H = 120$ GeV	no $\sqrt{\hat{s}}$ cut	$\sqrt{\hat{s}} > 210$ GeV	$\sqrt{\hat{s}} > 300$ GeV
$\sigma_S^{QCD}$ fb	10.6	7.0	4.0
$\sigma_S^{EW}$ fb	1.1	0.81	0.58
$\sigma_B$ fb/GeV	25.3	9.1	2.9

The reducible QCD background should be also suppressed by the  $\sqrt{\hat{s}}$  cut, even stronger than the irreducible one. Indeed, the subprocesses of reducible background have a similar diagram topology. So our arguments (see next section) should work in this case also. However, a shift to smaller  $\sqrt{\hat{s}}$  for the reducible background processes will be larger than for irreducible ones, because the energy of parton misidentified as a photon will be reconstructed with a much higher loss of energy in comparison with the photon radiated from the hard subprocess directly.

## 7. Angular distributions in the partonic c.m.s.

Useful information is provided by the spin structure of *in* and *out*-states. For the dominant subprocess  $gg \rightarrow H + g$  a set of possible *in* spin states does not include spin 1, while the spin of the *out*-state is determined by the gluon. It means, in particular, that the S-wave does not contribute here. At the same time for the background subprocesses  $gq \rightarrow \gamma + \gamma + q$  and  $q\bar{q} \rightarrow \gamma + \gamma + g$  the same spin configurations are possible for both *in* and *out* states. So, the jet angular distribution in the partonic c.m.s. should be different for the signal and the background.

In Fig. 5a we represent the angular distributions for the signal and background processes. Here  $\vartheta_{jet}^*$  is the jet scattering angle in the partonic c.m.s. The background curve has a bump

while the signal curve is smooth enough. In Figs. 5b and 5c the same distributions are shown when the  $\sqrt{\hat{s}}$  cut is applied. One can see that events from the central part are suppressed. Qualitative interpretation of this effect is given by the simple observation that the relative contribution of partial waves with higher angular momentum increases with the collision energy for processes with t-channel exchange of virtual particles. Thus, the contribution of S-wave in the background is relatively suppressed, substantiating the effect of the cut on partonic collision energy  $\sqrt{\hat{s}}$  discussed in the previous section.

It is clear that the angular distributions of photons from the signal and background processes in the partonic c.m.s. should be different. Indeed, photons from the Higgs decay (giving uniform angular distribution in the Higgs rest frame) are produced mostly in the direction opposite to the jet in the partonic c.m.s. At the same time photons radiated from the final quark in  $gg$  subprocesses, which give dominant contribution to the background, will be observed mainly at small angles with the jet. This effect is clearly seen in Fig. 6a, where the distributions in  $\vartheta_{g\gamma}^*$  (angle between the jet and the photon with smaller  $p_t$ ) are represented in partonic c.m.s. Let us now apply the  $\sqrt{\hat{s}}$  cut. The distributions in this case are represented in Figs. 6b and 6c. One can see that events at small angles  $\vartheta_{g\gamma}^*$  are suppressed affecting mainly the background distribution. This is qualitatively understood because events with small angle  $\vartheta_{g\gamma}^*$  correspond in average to smaller momentum of the Higgs boson or  $\gamma\gamma$  system. Indeed, for high enough velocity of the  $\gamma\gamma$  system the corresponding Lorentz boost will turn (almost) all photons in the directions opposite to the jet momentum. So, events where one photon is radiated in the jet hemisphere should have smaller  $\sqrt{\hat{s}}$  than events where both photons are radiated opposite to the jet. In particular, this effect gives us one more argument why the  $\sqrt{\hat{s}}$  cut suppresses the background stronger than the signal.

## 8. Estimates for the LHC detectors

In this section we give some estimates of the *Signal/Background* ratio and the signal significance for LHC detectors in the channel  $pp \rightarrow \gamma\gamma + jet$  using basic numbers from ATLAS and CMS Technical Design Reports [1, 2]. First, the efficiency of photon detection should be taken into account. This important instrumental parameter is expected to be  $\sim 80\%$  for both detectors, and it was obtained from the simulation of  $pp \rightarrow H \rightarrow \gamma\gamma$  events in the detectors. Second, the fiducial area cuts should be considered to exclude the regions of electromagnetic calorimeter where the performance decreases crucially. The corresponding efficiency per photon can be taken at the level 95% for ATLAS and 92.5% for CMS. Finally, let us consider the  $M_{\gamma\gamma}$  bin optimization which affects rather strongly the signal significance. At LHC low luminosity regime and for  $M_H = 100$  GeV the 80% signal events reconstruction efficiency corresponds to the  $M_{\gamma\gamma}$  mass bin of 3.1 GeV (resolution parameter  $\sigma_m = 1.1$  GeV) for ATLAS Lead-Liquid-Argon electromagnetic calorimeter [1]. For CMS PbWO<sub>4</sub> electromagnetic calorimeter [2] the mass resolution parameter  $\sigma_m = 0.65$  GeV assumes the mass bin  $\Delta M_{\gamma\gamma} = 1.9$  GeV with the reconstruction efficiency 73% in this window. For larger  $M_H$  the  $M_{\gamma\gamma}$  resolution is slightly worse. Let us take the values  $\Delta M_{\gamma\gamma} = 3.25$  GeV and 2.0 GeV if  $M_H = 120$  GeV, and  $\Delta M_{\gamma\gamma} = 3.4$  GeV and 2.1 GeV if  $M_H = 140$  GeV, for ATLAS and CMS  $M_{\gamma\gamma}$  bin, correspondingly.

Then, the QCD next-to-leading corrections should be taken into account. As we have mentioned above, these corrections are unknown for the processes discussed here. Some estimate may be possible since it was shown (see [12] and the references therein) that the NLO corrections to the  $gg$  fusion subprocesses in the  $pp \rightarrow \gamma\gamma + X$  inclusive channel increase the Higgs production cross section by a factor  $K \sim 1.6$ . One can hope that the corresponding  $K$ -factor in our case will be at least of the same value. Of course, it is very probable that the NLO corrections enhance somehow the rates of background processes as well. So, in the absence of theoretical results let us use in our case the factor  $K^{NLO} = 1.6$  both for the signal and background subprocesses.

Finally we get the following numbers in the case of **C2** basic kinematical cuts and applying

additional cut  $\sqrt{\hat{s}} > 300$  GeV:

Low luminosity	$M_H = 100$ GeV		$M_H = 120$ GeV		$M_H = 140$ GeV	
	ATLAS	CMS	ATLAS	CMS	ATLAS	CMS
$\sigma_S^{eff}$ fb	1.8	1.6	3.4	2.9	3.6	3.1
$\sigma_B^{eff}$ fb	6.6	3.8	8.9	5.2	12.3	7.2
$S/B$	1/3.7	1/2.5	1/2.7	1/1.8	1/3.4	1/2.3
$S/\sqrt{B}$ (30 fb $^{-1}$ )	3.8	4.3	6.2	7.0	5.6	6.3

## 9. Conclusions

The channel  $\gamma\gamma + jet$  with the jet transverse energy  $E_t > 30$  GeV and rapidity  $|\eta| < 4.5$  (thus involving forward hadron calorimeters) gives very promising discovery possibilities for the Higgs boson with a mass of 100-140 GeV during the LHC operation at a low luminosity of  $\sim 10^{33}$  cm $^{-2}$ s $^{-1}$ . For example, with an integrated luminosity of 30 fb $^{-1}$  about 100 signal events could be observed for  $M_H = 120$  GeV with a number of background events only 3 times higher in ATLAS and 2 times higher in CMS detector. These numbers demonstrate the main advantage of this channel in comparison with the inclusive reaction  $pp \rightarrow \gamma\gamma + X$ , namely significant improvement of the  $S/B$  ratio. The estimate of the reducible background using only isolation criteria shows that it is less than 20% of the irreducible background. Our results for the signal and background rates mean that the discovery level  $S/\sqrt{B} = 5$  for the signal significance will be achieved already with an integrated luminosity of 30 fb $^{-1}$  for  $M_H = 110 - 140$  GeV.

We found that the detection of jets with rapidities up to  $|\eta| = 4.5$  improves noticeably the signal significance. For example, 20-25% improvement can be achieved in comparison with the case when hard jets are only centrally produced ( $|\eta| < 2.4$ ,  $E_t^{jet} > 40$  GeV).

We demonstrated that sufficiently rich kinematics of the three particle final state allows to introduce new observable distributions, suitable for a better separation of the signal. Further improvement of the signal significance can be achieved by using the *jet* and *jet-photon* angular distributions in the reconstructed partonic c.m.s. These distributions can be also used for a further suppression of the reducible QCD background.

One should also note that in the present analysis we used parameters obtained from the simulation of the reaction  $pp \rightarrow \gamma\gamma + X$  in ATLAS and CMS detectors. However, the  $\gamma\gamma + jet$  kinematics is more preferable for the event reconstruction than in the inclusive case. Reconstruction of the jet in the hadronic calorimeter allows to determine more precisely the position of interaction vertex. Photons from the Higgs decay in  $\gamma\gamma + jet$  state are more energetic than for the inclusive channel. So the photon reconstruction efficiency and effective mass resolution used in our analysis probably are too pessimistic. From the experimental data processing point of view, additional event selection criterion (trigger condition) of a jet in the final state allows to restrict the number of diphoton events in comparison with the inclusive channel, providing opportunities for a more careful analysis at a better  $S/B$  ratio. Altogether these factors could give a sizeable improvement of the signal significance.

## Acknowledgements

We are grateful to E. Boos, D. Denegri, I. Goloutvine, M. Mangano, A. Nikitenko, A. Pukhov and A. Rozanov for many useful discussions.

This work was partially supported by the Russian Ministry of Science and Technologies, INTAS grant 97-2085 and the Russian Foundation for Basic Research (grants 98-02-17699 and 96-02-19773).

# References

- [1] ATLAS Calorimeter Performance, TDR-1, CERN/LHCC 96-40, December 1996.
- [2] CMS ECAL Technical Design Report, CERN/LHCC 97-33, CMS TDR 4, 15 December 1997.
- [3] R.K. Ellis, I. Hinchliffe, M. Soldate and J.J. van der Bij, Nucl. Phys. **B297** (1988) 221.
- [4] C. Kao, Phys. Lett. **B328** (1994) 420.
- [5] R.A. Alanakyan and V.H. Grabski, Preprint YerPHI 1496(13)-97 (1997); hep-ph/9711436.
- [6] U. Baur and F.W.N. Glover, Nucl. Phys. **B339** (1990) 38.
- [7] D. Rainwater and D. Zeppenfeld, Preprint MADPH-97-1023 (1997); hep-ph/9712271.
- [8] S. Abdullin et al, CMS TN/94-247 (1994), unpublished.  
CMS Technical Proposal, CERN/:HCC report 94-38 (1994).
- [9] M.N. Dubinin, V.A. Ilyin and V.I. Savrin, CMS NOTE 97/101 (1997), unpublished; hep-ph/9712335.
- [10] E.E. Boos, M.N. Dubinin, V.A. Ilyin, A.E. Pukhov, V.I. Savrin, Preprint INP MSU 94-36/358 and SNUCTP 94-116 (1994); hep-ph/9503280.  
P.A. Baikov et al, in: Proc. X Workshop QFTHEP-95 (Zvenigorod, September 1995), ed. B. Levtchenko and V. Savrin (MSU, Moscow, 1996) p.101; hep-ph/9701412.
- [11] V.A. Ilyin, D.N. Kovalenko and A.E. Pukhov, Int. J. Mod. Phys. **C6** (1996) 761.  
D.N. Kovalenko and A.E. Pukhov, Nucl. Instrum. and Methods **389** (1997) 299.
- [12] M. Spira, A. Djouadi, D. Graudenz and P.M. Zerwas, Nucl. Phys. **B453** (1995) 17.  
M. Spira, Preprint CERN-TH/97-68 (1997); hep-ph/9705337.
- [13] C.R. Schmidt, Phys. Lett. **B413** (1997) 391.
- [14] H.L. Lai et al. (CTEQ collaboration), Phys. Rev. **D55** (1997) 1280.
- [15] S.G. Gorishny, A.L. Kataev, S.A. Larin and L.R. Surguladze, Mod. Phys. Lett. **A5** (1990) 2703.  
N. Gray, D.J. Broadhurst, W. Grafe and K. Schilcher, Z. Phys. **C48** (1990) 673.
- [16] S. Dawson, Nucl. Phys. **B249** (1984) 42.  
G.L. Kane, W.W. Repko and W.B. Rolnick, Phys. Lett. **B148** (1984) 367.
- [17] P. Agrawal and S.D. Ellis, Phys. Lett. **B229** (1989) 145.  
R. Kleiss, Z. Kunszt and W.J. Stirling, Phys.Lett. **B253** (1991) 269
- [18] T. Sjostrand, Comp. Phys. Comm. **82** (1994) 74.

## Figure captions

Figure 1: Feynman diagrams for the QCD signal subprocesses: a)  $gg \rightarrow H + g$ , b)  $gq \rightarrow H + q$  and c)  $q\bar{q} \rightarrow H + g$ .

Figure 2: Feynman diagrams for the electroweak signal subprocesses with a)  $WW$  and  $ZZ$  fusion mechanisms of the Higgs boson production, b) associated  $HW$  and  $HZ$  production.

Figure 3: Feynman diagrams for the subprocesses a)  $gq \rightarrow \gamma + \gamma + q$  and b)  $q\bar{q} \rightarrow \gamma + \gamma + g$  contributing to the irreducible background.

Figure 4: Distributions in the parton c.m. energy  $\sqrt{\hat{s}}$  for the signal (S) (without EW contribution) and background (B) processes. Here  $M_H = 120$  GeV and the basic set of kinematical cuts **C2** is imposed. The  $\gamma\gamma$  invariant mass for the background is integrated over the 1 GeV bin.

Figure 5: Distributions in the jet angle in partonic c.m.s. for the signal (S) (without EW contribution) and background (B) processes in the case  $M_H = 120$  GeV. Upper plot is obtained with the basic set of kinematical cuts **C2**. Next plots show changes in this distribution when the  $\sqrt{\hat{s}}$  cut is applied. The  $\gamma\gamma$  invariant mass for the background is integrated over the 1 GeV bin.

Figure 6: Distributions in the angle between jet and the photon with smaller transverse momentum in partonic c.m.s. for signal (S) (without EW contribution) and background (B) processes in the case  $M_H = 120$  GeV. Upper plot is obtained with the basic set of kinematical cuts **C2**. Next plots show changes in this distribution when the  $\sqrt{\hat{s}}$  cut is applied. The  $\gamma\gamma$  invariant mass for the background is integrated over the 1 GeV bin.

# Figures

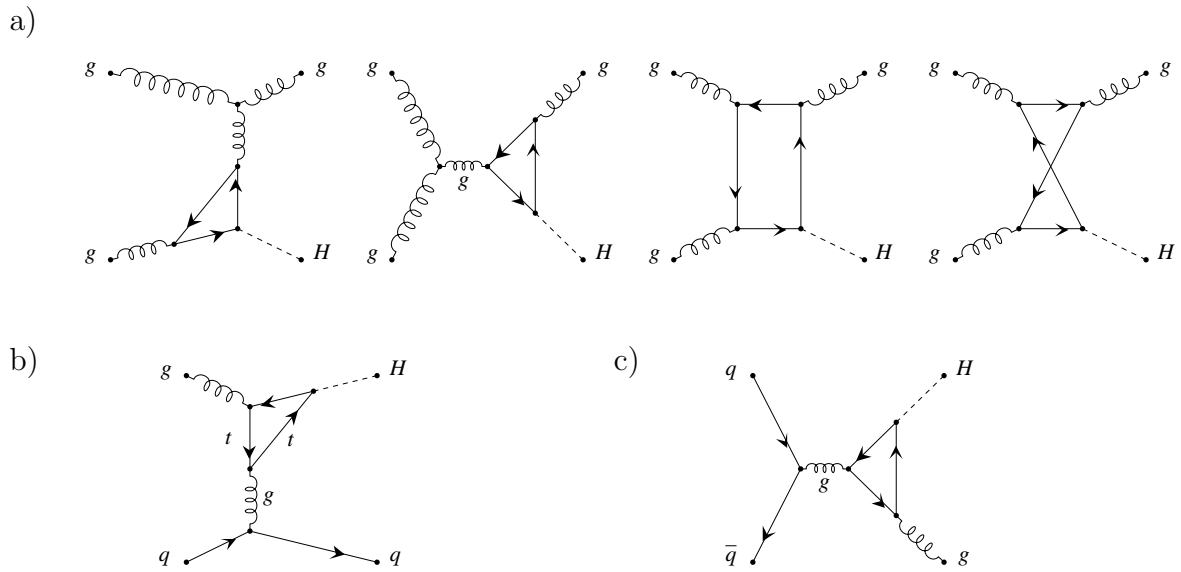


Figure 1:

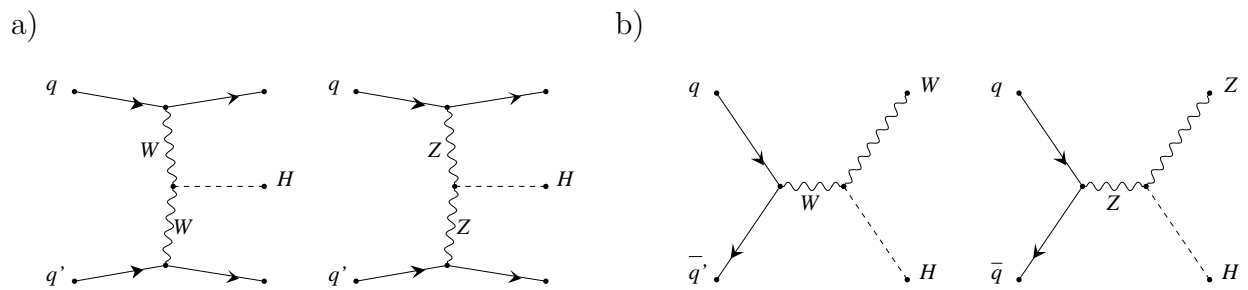
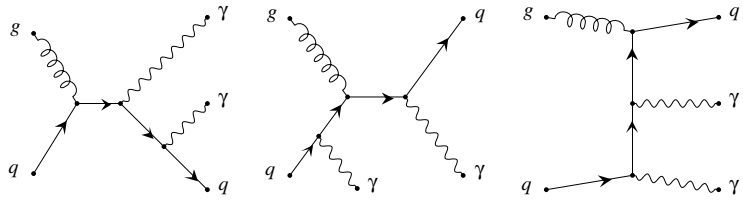


Figure 2:

a)



b)

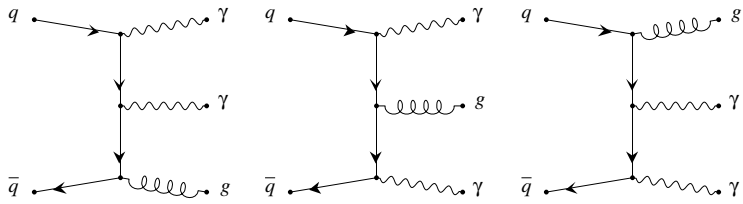


Figure 3:

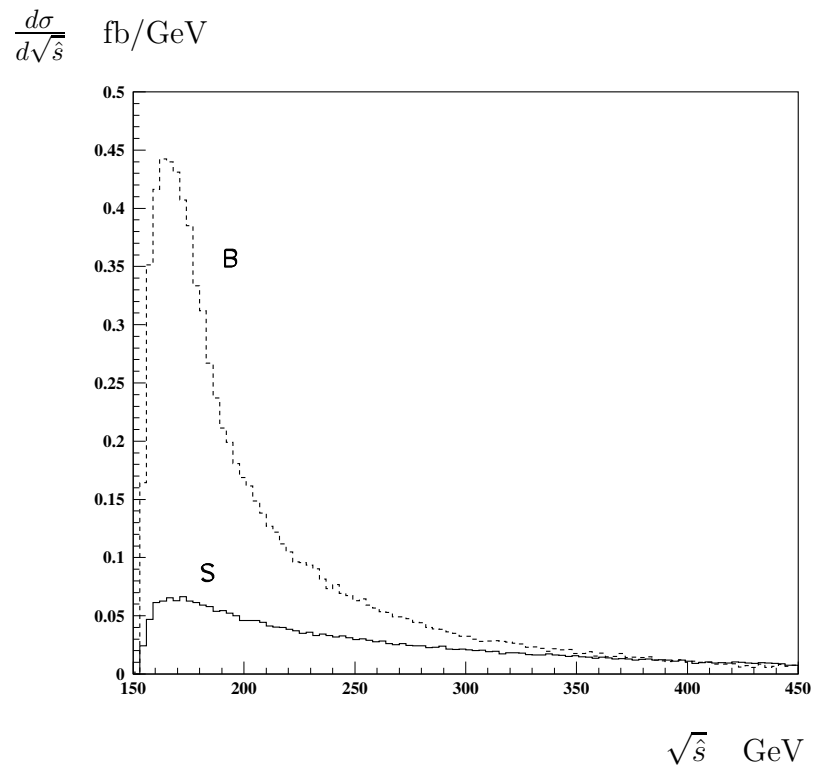


Figure 4:

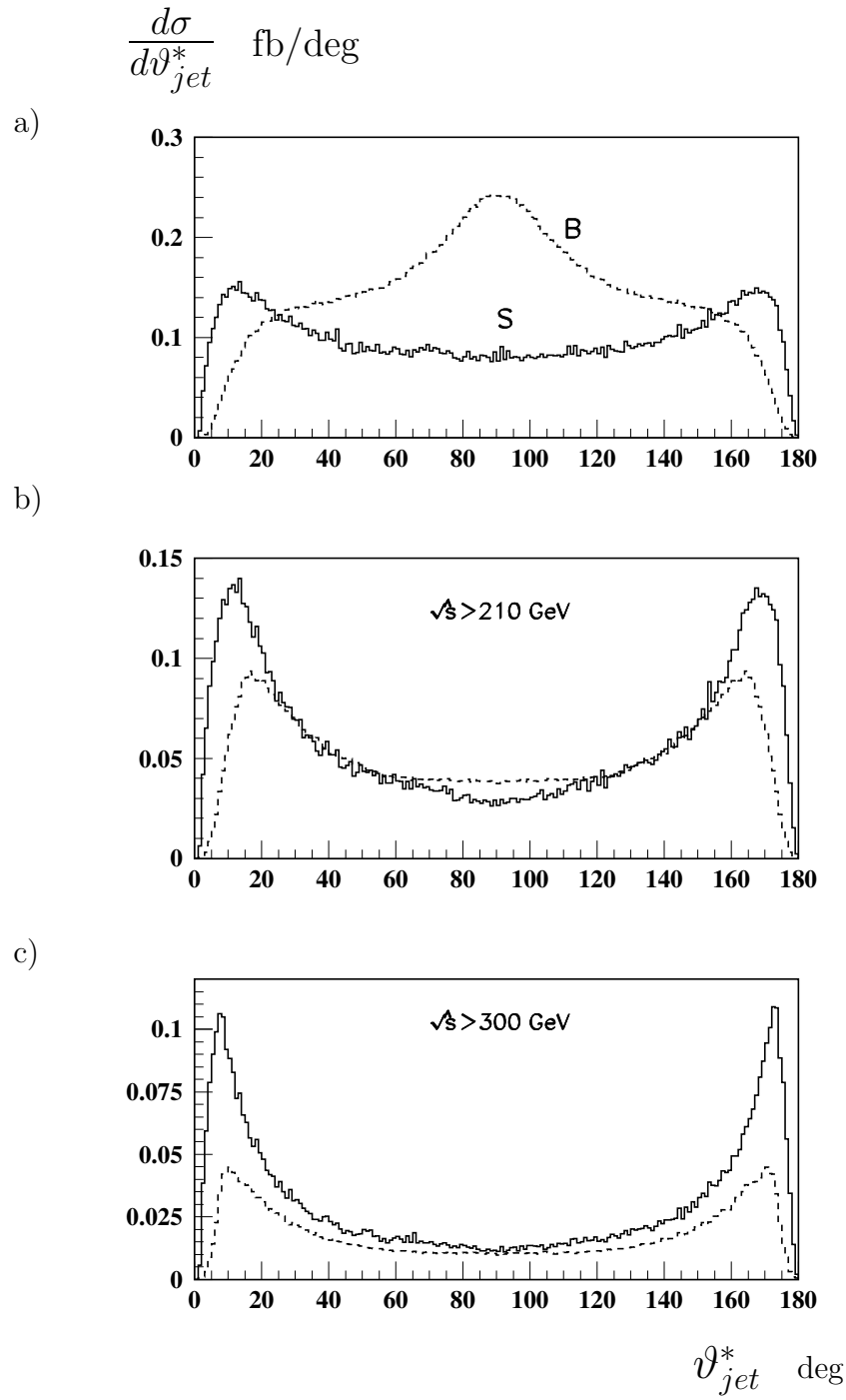


Figure 5:

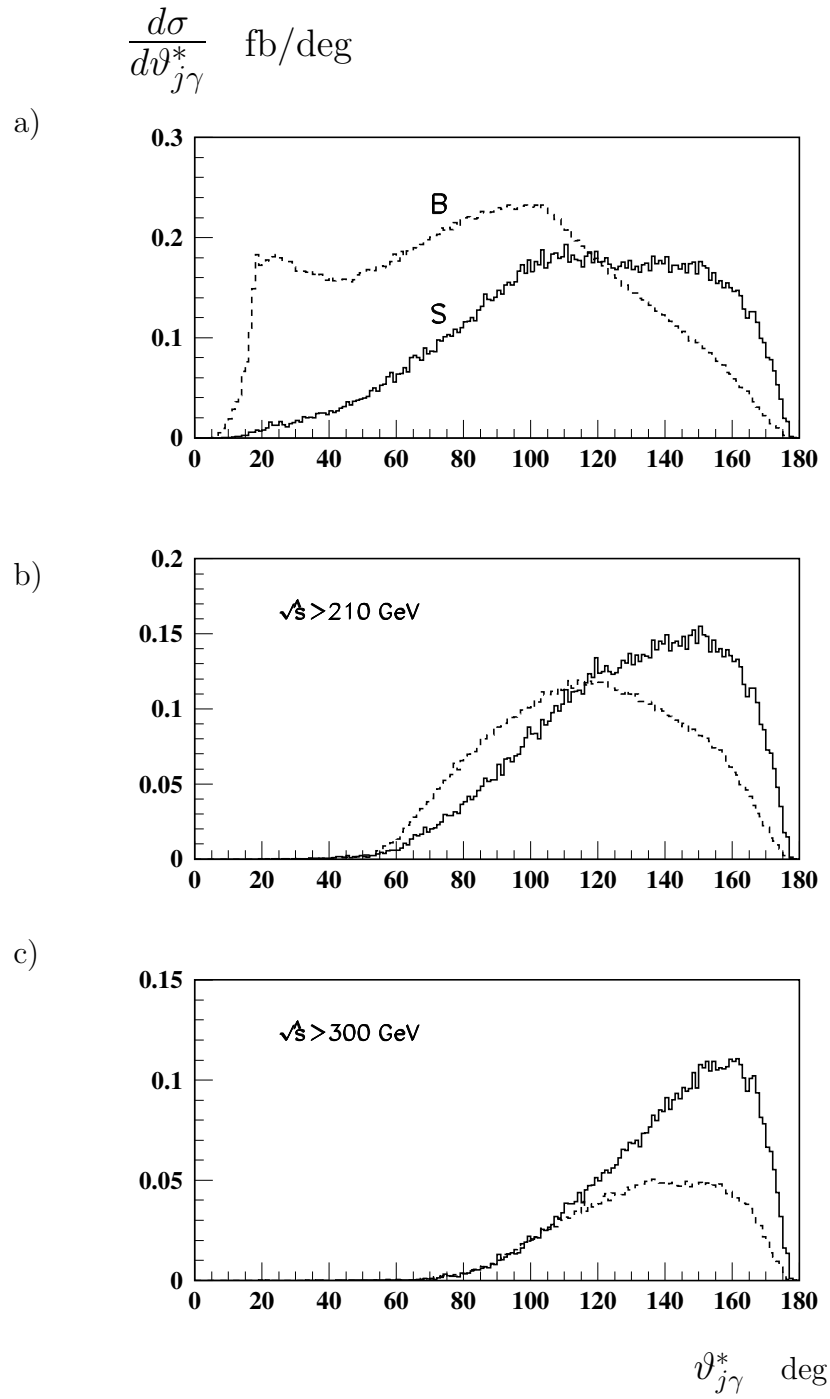


Figure 6: